Highlights of Spanish Astrophysics XI, Proceedings of the XV Scientific Meeting of the Spanish Astronomical Society held on September 4–9, 2022, in La Laguna, Spain. M. Manteiga, L. Bellot, P. Benavidez, A. de Lorenzo-Cáceres, M. A. Fuente, M. J. Martínez, M. Vázquez- Acosta, C. Dafonte (eds.), 2023

Testing the homogeneity of Type Ia Supernovae in the Near-infrared for accurate distance estimations.

Müller-Bravo T. E.[1,2], Galbany L.[1,2], Karamehmetoglu E.[3], Stritzinger M.[3], Burns C.[4], Phan K.[3,2], Iáñez-Ferres A.[1], Anderson J.[5], Ashall C.[6], Baron E.[7,8,9], Hoeflich P.[10], Hsiao E.[10], de Jaeger T.[6], Kumar S.[10], Lu J.[10], Phillips M.[11], Shahbandeh M.[10], Suntzeff N.[12], and Uddin S.[12,13]

[1] Institute of Space Sciences (ICE, CSIC), Campus UAB, Carrer de Can Magrans, s/n, E-08193 Barcelona, Spain
[2]Institut d'Estudis Espacials de Catalunya (IEEC), E-08034 Barcelona, Spain
[3]Department of Physics and Astronomy, Aarhus University, Ny Munkegade 120, DK-8000 Aarhus C, Denmark
[4]Observatories of the Carnegie Institution for Science, 813 Santa Barbara St., Pasadena, CA 91101, USA
[5]European Southern Observatory, Alonso de Córdova 3107, Casilla 19, Santiago, Chile
[6]Institute for Astronomy, University of Hawai'i, 2680 Woodlawn Drive, Honolulu, HI 96822, USA
[7]Department of Physics & Astronomy, University of Oklahoma, Norman, OK 73019 USA
[8]Department of Physics & Astronomy, George Washington University, Washington, DC USA
[9]Hamburger Sternwarte, Hamburg, Germany
[10]Department of Physics, Florida State University, 77 Chieftan Way, Tallahassee, FL 32306, USA
[11]Carnegie Observatories, Las Campanas Observatory, Casilla 601, La Serena, Chile
[12]George P. and Cynthia Woods Mitchell Institute for Fundamental Physics and Astronomy, Texas A&M University, Department of Physics and Astronomy, College Station, TX 77843, USA
[13]Centre for Space Studies, American Public University System, 111 W. Congress Street, Charles Town, WV 25414, USA

Abstract

Since the discovery of the accelerating expansion of the Universe more than two decades ago, Type Ia Supernovae (SNe Ia) have been extensively used as standardisable candles in the optical. However, SNe Ia have shown to be more homogeneous in the near-infrared (NIR), where the effect of dust extinction is also attenuated. In this work, we explore the possibility of using a low number of NIR observations for accurate distance estimations, given the homogeneity at these wavelengths. We found that one epoch in J and/or H band, plus good gr-band coverage, gives an accurate estimation of peak magnitudes in the J and H bands. The use of a single NIR epoch only introduces a small additional scatter for epochs around the time of B-band peak magnitude. These results provide confidence for our FLOWS project that is aimed at using SNe Ia with public ZTF optical light curves and few NIR epochs to map out the peculiar velocity field of the local Universe. This will allow us to determine the distribution of dark matter in our own supercluster, Laniakea, and to test the standard cosmological model by measuring the growth rate of structures, parameterised by fD, and the Hubble-Lemaître constant, H_0.

1 Introduction

The expansion rate of the Universe, parameterised by the Hubble-Lemaître parameter, H(z), varies across cosmic time. In the last few years, there has been tremendous effort to measure the local value, known as the Hubble-Lemaître constant (H_0), with extremely high precision ($< 2\%$ uncertainty;[37]). Recent results have further increased the discrepancy in the value of H_0 between the local distance ladder ($H_0 = 73.04 \pm 1.04\,\mathrm{km\,s^{-1}\,Mpc^{-1}}$, baseline with systematics; [37]) and the cosmic microwave background (CMB; $H_0 = 67.4 \pm 0.5\,\mathrm{km\,s^{-1}\,Mpc^{-1}}$;[34]) measurements, colloquially known as the 'Hubble tension', to 5σ (however, see [15, 22, 24] for some alternative local measurements). This discrepancy possibly hints towards new physics beyond the standard cosmological model, or alternatively, unaccounted systematic effects (see [11] for a recent review on the Hubble tension).

In the local Universe, the recession velocities measured from galaxies are affected by a combination of the expansion of the Universe and the gravitational pull of other adjacent galaxies. The measurement of these peculiar velocities is critical for two main reason. First, cosmological analyses with Type Ia Supernovae (SNe Ia) rely on discerning the contribution of peculiar velocities to isolate the cosmological redshift. Secondly, peculiar velocities can be used to inferred the matter-density distribution in the local Universe ([29]), including our own supercluster, Laniakea (e.g. [43]). The latter provides a direct measurement of the growth-rate of structure, which can be compared to estimates from the early Universe (e.g. [27]).

Current measurements of peculiar velocities often rely on methods such as the Fundamental-Plane and Tully-Fisher relations (e.g. [44]), which provide distances with relatively large uncertainties (with an rms of $\sim 20 - 30\%$ per galaxy) and only reach out to $z \sim 0.05$, standing

in the way of the study of the peculiar velocities at further distances. Therefore, there is a lack of higher-precision methods that can also extend to further redshifts for the estimation of distances in the local Universe.

Since the discovery of the accelerating expansion of the Universe more than two decades ago ([36, 30]), SNe Ia have been extensively used as cosmological distance indicators. In the optical, their light curves can be standardised through empirical relations between their peak brightness, stretch (e.g. [38, 35, 31]), and colour ([42]). In addition, SNe Ia are brighter in the optical (where detectors are larger as well), compared to other wavelengths, making them easier to observe. Therefore, cosmological analyses with SNe Ia (e.g. [4, 39, 1]) commonly focus on optical wavelengths and rely on light-curve fitters, such as SALT2 ([18, 19]), for the estimation of their light-curve parameters. Moreover, SNe Ia in the optical have recently been used to estimate the growth-rate of structures (e.g. [5, 40]).

SNe Ia were first proposed as distance indicators in the near-infrared (NIR) around four decades ago ([12, 13], but also see [28]), where they seem to be true 'standard candles' (as opposed to 'standardisable candles' in the optical). In other words, an estimation of the NIR peak magnitudes is all that is needed to measure distances. The NIR light curves of SNe Ia present lower intrinsic dispersion than the optical light curves and have the advantage of being less affected by dust extinction, which makes them exceptional for measuring cosmological distances (e.g. [25, 46, 14, 3, 32, 45, 16, 23]). Moreover, the NIR light curves of SNe Ia have already been used to constrain H_0 to a few percent (e.g. [8, 10]).

The low intrinsic dispersion of SNe Ia in the NIR raises the the possibility of using them to achieve accurate cosmography by measuring peculiar velocities of local galaxies, reaching out to $z \sim 0.1$ or even beyond. However, the sample of SNe Ia observed in the NIR is currently low due to several factors: low NIR detector sensitivity in the past; SNe Ia are fainter at these wavelengths, where the sky brightness dramatically decreases the contrast for the (SN) observations, thus needing to integrate for longer; and the number of facilities with NIR instruments (compared to optical ones) is low. However, by taking advantage of the exceptional homogeneity of the SNe Ia in the NIR, we can possibly reconstruct their light curves with just a few photometric data points (e.g. [25]), increasing the total number of observed objects.

Given the large stream of optical photometry publicly provided by the Zwicky Transient Facility (ZTF; [17]), which works as a precursor and testing ground for LSST, hundreds to thousands of SNe Ia are being followed-up with high-cadence (average of 2 days) *gr*-bands photometry. Thus, ZTF can provide the optical data coverage while NIR photometry can be obtained with other facilities. This work aims to test how accurately we can retrieve NIR peak magnitudes with well-covered optical light curves and few NIR epochs for distance estimations. Our results will give assurance to use SNe Ia with public ZTF *gr*-band light curves with sparse data in the NIR to reconstruct the cosmography of our local supercluster, measure the growth-rate of structure and H_0, and test ΛCDM and alternative cosmological models. In the future, this can be extended to use optical data from the Rubin Observatory Legacy Survey of Space and Time (LSST) and NIR data from telescopes such as the Roman Space Telescope and James Webb Space Telescope.

2 Data and method

We use the Carnegie Supernova Project (CSP; [20]) sample as it is one of the most comprehensive samples of SNe Ia with extensive *uBgVriYJH* (optical to NIR) coverage and well-understood magnitude systems to date. The data from CSP-I consists of three data releases (DRs) described in [9](DR1), [41](DR2) and [26](DR3), while the data from CSP-II are described in [33] and [21]. CSP-II does not have a public DR to date, but one is in progress (Suntzeff et al., in prep.). We include all the 134 SNe Ia from CSP-I and 202 from CSP-II (the cosmology sub-sample from [33]). Thus, the CSP sample we use consists of a total of 336 SNe Ia.

As CSP observations have used different filters and telescopes throughout the different campaigns, we apply S-corrections ([41]) to work in a single magnitude system, simplifying the handling of data. This is specifically useful for those CSP-I SNe with multiple V, Y, or J bands, and for combining SNe from CSP-I and CSP-II.

To fit the SNe Ia, we use SNooPy ([6]) with the *max_model* model, as we require measurements of the peak magnitudes in J and H ($J_{\max}$ and $H_{\max}$, respectively). The resulting fits provide the following output parameters: $T_{\max}$, s_{BV}, and $x_{\max}$, where $T_{\max}$ is the time of B-band peak magnitude, s_{BV} is the 'colour stretch' parameter as defined in [7] and $x_{\max}$ represents the peak magnitude in x-band, for each of the observed filters. We note that the multi-colour light-curve templates (optical to NIR) are driven by the values of $T_{\max}$ and s_{BV}. All magnitudes presented are in the CSP natural system and the reported uncertainties from SNooPy fits are statistical uncertainties only.

As not all CSP SNe are useful for the purpose of this work, we proceeded to apply some cuts to the initial sample. We only used SNe Ia labelled as 'normal' according to [26] and [2]. We then proceed to remove any SN without g, r, J, or H bands, as these are strictly required for our analysis: g and r being the bands used by ZTF while J and H being the NIR bands commonly available. The Y band is not included as catalogues of standard stars for this band are not available for the whole sky, which are needed for the calibration. The next cut requires the SN to have coverage of the optical peak as the estimation of $T_{\max}$ is fundamental when fitting the light curves of SNe Ia. For this, we need to have one or more photometric points at least two days before and two days after $T_{\max}$ in B, g, V, or r bands, providing an accurate estimation of the location of the peak. Finally, we require at least one photometric point before and after the time of $J_{\max}$ and $H_{\max}$, as precise measurements of these are needed.

3 Simulations

Given that we want to replicate what real observations would be (i.e. optical bands well covered with few NIR data points), the simulations consist of taking the complete gr-band light curves, plus n epochs of coeval J- and $\tilde{}$band photometric points, for $n = 1, 2$, and 3. We note that we are sampling from the available photometry (henceforth referred to as 'simulations' in this paper). Combinations without repetition of the JH-band photometry are

used for this The resulting simulations are then fit, using SNooPy and the output parameters saved for a later comparison.

Assuming that SNe Ia are standard candles in the NIR, peak NIR magnitudes can be directly used to estimate distances without further corrections (e.g. from stretch or colour). Thus, our main interest is to see how well we can measure $J_{\rm max}$ and $H_{\rm max}$ using just a few NIR photometric points. However, the retrieved peak magnitudes highly depend on the time of the observations with respect to $T_{\rm max}$. We therefore define three different metrics to understand what type of observations are best at obtaining accurate $J_{\rm max}$ and $H_{\rm max}$ measurements:(i) time of the closest J/H epoch with respect to $T_{\rm max}$; (ii) mean time of the J/H epochs with respect to $T_{\rm max}$; and (iii) difference between the earliest and latest (i.e. range) J/H epochs. Note that in the case of the simulations with only one epoch ($n = 1$), metrics (i) and (ii) are the same, while (iii) is not calculated. Also note that these metrics are defined in the restframe, i.e. epochs are corrected for time dilation using the SN redshift.

In Figure 1, we show $J_{\rm max}$ residuals between the simulations and the reference sample (using all bands) as a function of metric (i), for simulations with *grJH* bands and $n = 1$. From this comparison, we see that the scatter in the residuals tends to be smaller around $T_{\rm max}$, with the smallest scatter before $T_{\rm max}$, and increases at later epochs. In general, the scatter is smaller for the H band (not shown in the figure) compared to the J band. This is consistent with what has been found in other works (e.g. [**?**]). Additionally, we note that offsets in $J_{\rm max}$ and $H_{\rm max}$ tend to be larger where the NIR light-curve templates have a larger gradient or slope.

As we are aiming to reduce the scatter, ideally, we would need data around $T_{\rm max}$. Unfortunately, as it is hard to obtain photometric data at specific epochs due to different constraints (weather, time, allocation, etc.), we have to look for a time window with a large-enough range. We noticed that a time range between -5 to 15 days with respect to $T_{\rm max}$ possess a relatively low scatter in $J_{\rm max}$ and $H_{\rm max}$. The weighted mean (Δ) and weighted standard deviation (σ) of the residuals in this time window are $\Delta = 0.004\,$mag and $\sigma = 0.047\,$mag, and $\Delta = -0.006\,$mag and $\sigma = 0.053\,$mag, for $J_{\rm max}$ and $H_{\rm max}$, respectively.

4 Near-infrared distances

The final step in this work is to calculate the precision in the distance estimations from the simulations. Assuming that SNe Ia are standard candles in the NIR, the peak apparent magnitude is the only parameter necessary to calculate distances and its uncertainty is directly propagated to the measured distance:

$$\mu = m_{\rm max} - M, \tag{1}$$

where μ is the distance modulus, $m_{\rm max}$ is the peak apparent magnitude in a NIR band (e.g. $J_{\rm max}$ or $H_{\rm max}$) and M is the peak absolute magnitude in that same band. To calculate distances, a cosmological model needs to be fitted. For simplicity, we assume a flat ΛCDM cosmology and fix the value of M ($M_J = M_H = -18.5\,$mag), fitting only H_0 and the intrinsic

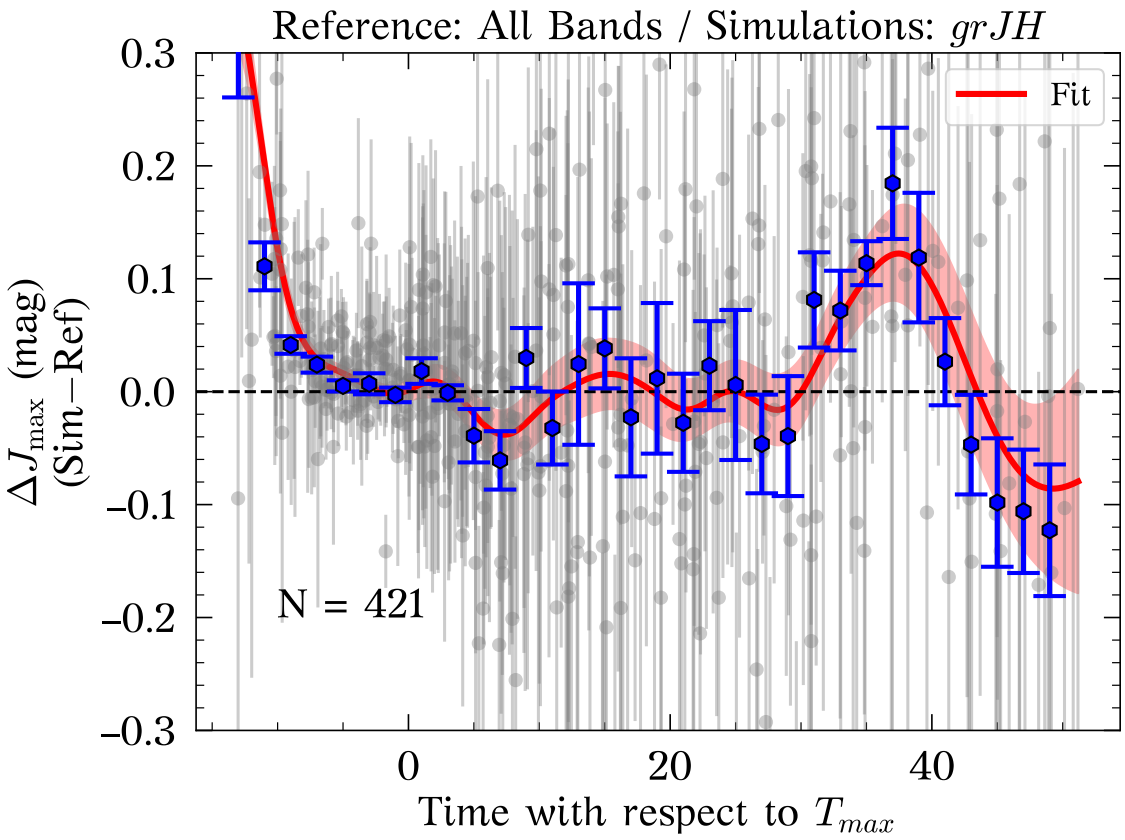

Figure 1: $J_{\rm max}$ residuals, between simulations with coeval coeval J-band epoch and reference value. The weighted mean and uncertainty on the weighted mean in bins of two days are shown in blue. A "correction snake" and its uncertainty are calculated by fitting the residuals with Gaussian Process (red line and shaded region), while N is the total number of simulations.

dispersion of SNe Ia ($\sigma_{\rm int}$). Only SNe at $z > 0.01$ are used as the contribution from peculiar velocities is relatively small at these redshifts. This reduces our reference sample to 36 objects. The resulting Hubble diagram in J band is shown in Figure 2 (red circles). The Hubble residuals have an rms of 0.166 mag, while $\sigma_{\rm int} = 0.14$ mag was obtained.

Using the simulations with phase between −5 days and 15 days, where a low scatter in $J_{\rm max}$ was found (see the previous section), an rms of 0.180 mag is obtained. Although the simulations have larger scatter than the reference sample, the difference is relatively small (0.014 mag). In the case of the H band, the reference sample and the simulations have Hubble residuals rms of 0.149 mag and 0.147 mag, respectively. The rms values are very similar, being slightly smaller for the simulations (a negligible difference of 0.002 mag).

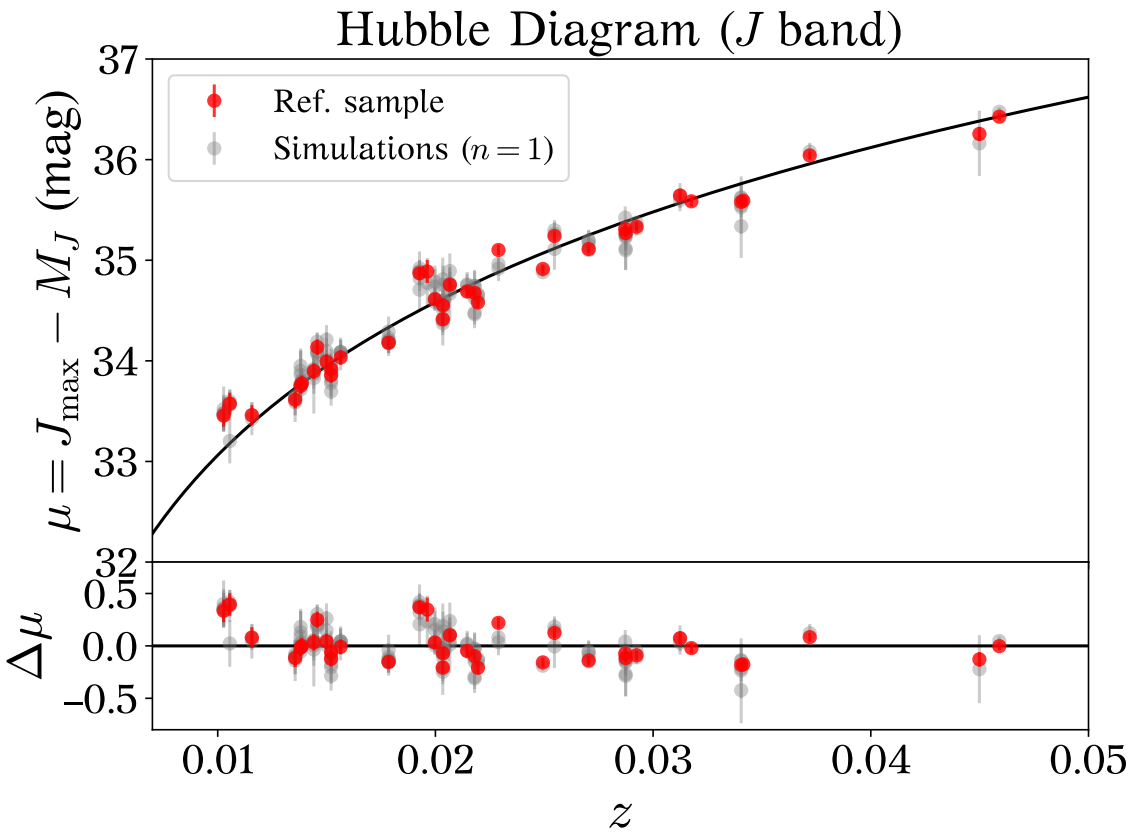

Figure 2: Hubble diagram in J-band. Only SNe Ia with $z > 0.01$ were used as the contribution from peculiar velocities is relatively small at these redshifts. The reference sample was used to fit H_0 and the intrinsic dispersion ($\sigma_{\rm int}$), keeping the peak absolute magnitude in J band ($M_J = -18.5$ mag) fixed. The rms for the reference sample (red) and the simulations with $n = 1$ (grey) are 0.166 mag and 0.180 mag, respectively.

Acknowledgments

TEMB acknowledges financial support from the Spanish Ministerio de Ciencia e Innovación (MCIN), the Agencia Estatal de Investigación (AEI) 10.13039/501100011033 under the PID2020-115253GA-I00 HOSTFLOWS project, from Centro Superior de Investigaciones Científicas (CSIC) under the PIE project 20215AT016 and the I-LINK 2021 LINKA20409, and the program Unidad de Excelencia María de Maeztu CEX2020-001058-M.

References

[1] Abbott, T., Allam, S., Andersen, P. 2019 ApJ, 872L, 30A

[2] Ashall, C., Lu, J., Burns, C. 2020 ApJ, 895L, 3A

[3] Barone-Nugent, R., Lidman, C., Wyithe, J. 2012 MNRAS, 425, 1007B
[4] Betoule, M., Kessler, R., Guy, J. 2014 A&A, 568A, 22B
[5] Boruah, S., Hudson, M., Lavaux, G. 2020 MNRAS., 498, 2703B
[6] Burns, C., Stritzinger, M., Phillips, M. 2011 AJ, 141, 19B
[7] Burns, C., Stritzinger, M., Phillips, M. 2014 ApJ, 789, 32B
[8] Burns, C., Parent, E., Phillips, M. 2018 ApJ, 869, 56B
[9] Contreras, C., Hamuy, M., Phillips, M. 2010 AJ, 139, 519C
[10] Dhawan, S., Jha, S., Leibundgut, B. 2018 A&A, 609A, 72D
[11] Di Valentino, E., Mena, O., Pan, S. 2021 CQGra, 38o3001D
[12] Elias, J., Frogel, J., Hackwell, J. 1981 ApJ, 251L, 13E
[13] Elias, J., Matthews, K., Neugebauer, G. 1985 ApJ, 296, 379E
[14] Freedman, W., Burns, C., Phillips, M. 2009 ApJ, 704, 1036F
[15] Freedman, W., Madore, B., Hatt, D. 2019, ApJ, 882, 34F
[16] Friedman, A., Wood-Vasey, W., Marion, G. 2015 ApJS, 220, 9F
[17] Graham, M., Kulkarni, S., Bellm, E. 2019 PASP, 131g8001G
[18] Guy, J., Astier, P., Nobili, S. 2005 A&A, 443, 781G
[19] Guy, J., Astier, P., Baumont, S. 2007 A&A, 466, 11G
[20] Hamuy, M., Folatelli, G., Morrell, N. 2006 PASP, 118, 2H
[21] Hsiao, E., Phillips, M., Marion, G. 2019 PASP, 131a4002H
[22] Huang, C., Riess, A., Yuan, W. 2020 ApJ, 889, 5H
[23] Johansson, J., Cenko, S., Fox, O. 2021 ApJ, 923, 237J
[24] Khetan, N., Izzo, L., Branchesi, M. 2021 A&A, 647A, 72K
[25] Krisciunas, K., Phillips, M., Suntzeff, N. 2004 ApJ, 602L, 81K
[26] Krisciunas, K., Contreras, C., Burns, C. 2017 AJ, 154, 211K
[27] Linder, E. 2005 PhRvD, 72d3529L
[28] Meikle, W. 2000 MNRAS, 314, 782M
[29] Peebles, P. 1976 ApJ, 205, 318P
[30] Perlmutter, S., Aldering, G., Goldhaber, G. 1999 ApJ, 517, 565P
[31] Phillips, M. 1993ApJ, 413L., 105P
[32] Phillips, M. 2012 PASA, 29, 434P
[33] Phillips, M., Contreras, C., Hsiao, E. 2019 PASP, 131a4001P
[34] Planck Collaboration 2020, A&A, 641A, 6P
[35] Pskovskii, I. 1977 SvA, 21, 675P
[36] Riess, A., Filippenko, A., Challis, P. 1998 AJ, 116, 1009R

[37] Riess, A., Casertano, S., Yuan, W. 2021, ApJ, 908L, 6R

[38] Rust, B. 1974 PhDT, 7R

[39] Scolnic, D., Jones, D., Rest, A. 2018 ApJ, 859, 101S

[40] Stahl, B., de Jaeger, T., Boruah, S. 2021 MNRAS, 505, 2349S

[41] Stritzinger, M., Phillips, M., Boldt, L. 2011 AJ, 142, 156S

[42] Tripp, R. 1998 A&A, 331, 815T

[43] Tully, R., Courtois, H., Hoffman, Y. 2014 Natur., 513, 71T

[44] Tully, R., Courtois, H., Sorce, J. 2016 AJ, 152, 50T

[45] Weyant, A., Wood-Vasey, W., Allen, L. 2014 ApJ, 784, 105W

[46] Wood-Vasey, W., Friedman, A., Bloom, J. 2008 ApJ, 689, 377W